CTLA-4 nanovesicles disrupt dendritic cell-driven CD8 T cell priming for myocardial infarction therapy

Shengnan Wang, Mengting Li, Han Shen, Wenjing Zhou, Jiuyuan Sun, Qingsong Tang, Hongman Liu, Wencheng Zhang, Zhenya Shen, Weiqian Chen

PII: S0168-3659(25)00890-9

DOI: https://doi.org/10.1016/j.jconrel.2025.114277

Reference: COREL 114277

To appear in: *Journal of Controlled Release*

Received date: 24 June 2025

Revised date: 25 September 2025

Accepted date: 26 September 2025

Please cite this article as: S. Wang, M. Li, H. Shen, et al., CTLA-4 nanovesicles disrupt dendritic cell-driven CD8 T cell priming for myocardial infarction therapy, *Journal of Controlled Release* (2024), https://doi.org/10.1016/j.jconrel.2025.114277

CTLA-4 nanovesicles disrupt dendritic cell-driven CD8 T cell priming for myocardial infarction therapy

Shengnan Wang[1, #], Mengting Li[1, #], Han Shen[1, #], Wenjing Zhou[1, 4, #], Jiuyuan Sun[1], Qingsong Tang[1], Hongman Liu[1, 3], Wencheng Zhang[2], Zhenya Shen[1, *], Weiqian Chen[1, *]

[1] Department of Cardiovascular Surgery of the First Affiliated Hospital & Institute for Cardiovascular Science, Suzhou Medical College of Soochow University, Soochow University, Suzhou, China.

[2] State Key Laboratory for Innovation and Transformation of Luobing Theory, Key Laboratory of Cardiovascular Remodeling and Function Research, Chinese Ministry of Education, Chinese National Health Commission and Chinese Academy of Medical Sciences, Department of Cardiology, Qilu Hospital of Shandong University, Jinan, China

[3] Department of Cardiovascular Medicine, The Affiliated Taian City Central Hospital of Qingdao University, Taian, China

[4] School of Life Science, Tianjin University, Tianjin, China

[#] These authors contributed equally to this paper

Corresponding authors: Weiqian Chen (86-188-6210-9196, chenweiqian@suda.edu.cn) and Zhenya Shen (86-512-6797-2066, uuzyshen@aliyun.com)

Abstract

Myocardial infarction (MI) remains a formidable global health challenge, as current therapies are hindered by excessive inflammation that exacerbates cardiac dysfunction and accelerates disease progression. Cytotoxic T-lymphocyte antigen 4 (CTLA-4) and CD28 are T-lymphocyte receptors with opposing roles in T-cell activation: CD28 binding to CD80/CD86 ligands on dendritic cells (DCs) mediates co-stimulation, whereas CTLA-4 engagement delivers inhibitory signals. In our present study, mannosylated cytotoxic T-lymphocyte antigen 4 (CTLA-4)-presenting small extracellular vesicles (CM@sEVs) were engineered for targeted MI therapy. By disrupting the CD80/86-CD28 costimulatory signaling, these CM@sEVs counteract dendritic cell (DC)-driven $CD8^+$ T cell priming, thereby mitigating ischemic immunopathology while supporting myocardial repair. Notably, distinct from existing T-cell modulatory therapies, our CM@sEVs uniquely reshape *in vivo* T-cell dynamics directly through DC-dependent mechanisms, offering a precise and stable strategy for ischemic cardiomyopathy.

Key Words

myocardial infarction; inflammation; extracellular vesicle; dendritic cell; T cell; CTLA-4

Introduction

As a critical cardiovascular event, myocardial infarction (MI) continues to impose substantial health risks worldwide [1]. Post-MI ischemic injury prompts the activation of a broad spectrum of innate and adaptive immune cells in the affected myocardium. In our prior study, we analyzed publicly available single-cell sequencing data from ischemic murine hearts, uncovering highly heterogeneous T lymphocyte populations and clusters of hyper-activated, proliferative $CD8^+$ T cells [2]. While appropriately regulated local inflammatory responses are crucial for clearing cellular debris and initiating myocardial repair, excessive $CD8^+$ T cell inflammation can lead to uncontrolled immunopathology, inefficient healing, and adverse remodeling [3]. Initiation of T-cell immunity is primarily orchestrated by the interaction between mature dendritic cells (DCs) and naive T cells, with DCs presenting MHC molecules and delivering CD80/86 co-stimulatory signals [4]. Consequently, targeting DC-driven $CD8^+$ T cell priming emerges as a promising therapeutic strategy for MI management.

Cytotoxic T-lymphocyte antigen 4 (CTLA-4 or CD152) and CD28 are homologous receptors on T lymphocytes that play opposing roles in T cell activation. CD28 engages with CD80/CD86 ligands on the DC surface, mediating T-cell co-stimulation. Conversely, interaction between CTLA-4 and CD80/CD86 inhibits T-cell responses by delivering negative regulatory signals [5, 6]. While both receptors share CD80/CD86 as ligands, CTLA-4 competes with CD28, effectively reducing the availability of these ligands for co-stimulation and thereby suppressing T cell activation [7, 8]. Therefore, targeting the CD28-CD80/86 co-stimulatory axis via CTLA-4 represents a promising therapeutic strategy for blocking DC-driven $CD8^+$ T cell priming.

Extracellular vesicles (EVs) are nanoscale membranous particles classically categorized into three subtypes by size, biogenesis pathway, and biomolecular composition: small EVs (sEVs, 40-200 nm; namely exosomes), microvesicles (50-2000 nm), and apoptotic bodies (500-4000 nm) [9]. By incorporating surface decoration, EVs have expanded their biomedical applications [10, 11]. Herein, we established small EVs (<200 nm) [12] presenting membranous CTLA-4 (C@sEV) as a potent “immunological intervenor” to counteract DC-driven $CD8^+$ T cell priming. Recent investigations have highlighted glycan modifications for targeted delivery to DCs [13-16]. Accordingly, mannosylated C@sEVs, termed CM@sEVs, were developed to exploit the abundant mannose receptors on DCs, enhancing their targeting efficiency. Importantly, our CM@sEVs

effectively inhibit DC-driven CD8$^+$ T cell priming while concurrently mitigating *in vivo* ischemic immunopathology and facilitating myocardial tissue repair (Scheme 1). In contrast to conventional T cell modulatory therapies, CM@sEVs function through DC-dependent mechanisms, offering a straightforward, stable, and safe therapeutic strategy for ischemic cardiomyopathy.

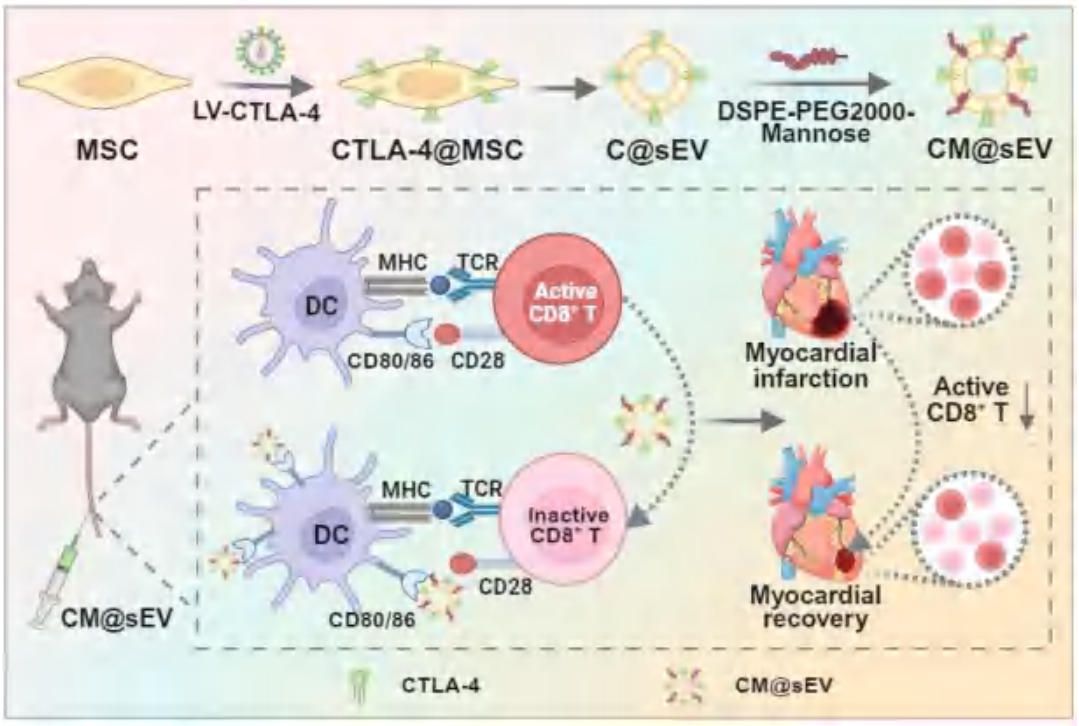

Scheme 1. Schematic model illustrating CM@sEV therapy for inhibiting DC-initiated CD8$^+$ T priming during MI. Mannosylated CTLA-4-presenting sEVs (CM@sEVs) were engineered as indicated. By disrupting CD80/86-CD28 co-stimulatory interaction, these CM@sEVs effectively restrained DC-driven CD8$^+$ T cell priming, thereby alleviating ischemic immunopathology and conferring cardiac recovery. Created in BioRender. Shengnan, W. (2025) https://BioRender.com/gqefnrl.

Results and discussion

Establishment and characterization of CM@sEVs

To generate CTLA-4-presenting sEVs (C@sEVs), murine MSCs were transduced with lentivirus encoding mouse CTLA-4-FLAG fusion protein and EGFP, yielding CTLA-4@MSCs. Small EVs were harvested from their culture medium and surface-modified with mannose (CM@sEVs) to enhance DC targeting (Figure 1A). MSC identity was confirmed through flow cytometry, revealing a CD29-positive, but CD45-, CD11b-, and CD117-negative phenotype (Figure S1). Morphologically, CTLA-4@MSCs displayed the expected spindle-shaped or irregular triangular structure with strong cytosolic EGFP fluorescence (Figure 1B), indicative of successful transduction. Additionally, flow cytometry demonstrated striking enhancement in CTLA-4 protein levels in CTLA-4@MSCs (Figure 1C&D). Finally, surface expression of CTLA-4 was validated by co-localization of the FLAG tag with membrane-bound lectin (Figure 1E), suggesting both robust overexpression and proper integration of CTLA-4 at the membrane level.

Morphologically, all sEVs were physically homogenous with classic membranous vesicle architecture (Figure 1F), with size distribution spanning from 100 to 150 nm (Figure 1G). Electrokinetic measurements demonstrated zeta potentials ranged from -30 to -20 mV (Figure 1H), coupled with polydispersity indices (PDI) below 0.4 (Figure 1I), collectively indicating favourable colloidal stability. Crucially, the absence of cytoplasmic or nuclear contaminants was confirmed by the diploid expression of Histone H3 and GAPDH (Figure 1J), further validating sEV purity. Biologically, all sEVs exhibited characteristic expression of CD63 and CD81 (Figure 1K-O), affirming their EV identity. Expectedly, both C@sEVs and CM@sEVs displayed elevated membranous CTLA-4 expression (Figure 1P&Q), while lacking cytosolic EGFP fluorescence (Figure 1R&S). To indirectly evaluate the stability of surface modifications, we conjugated DSPE-PEG2000-FITC onto sEVs and compared the FITC fluorescence intensity between freshly prepared samples and those stored at -80°C for one month. Notably, latex bead-based flow cytometry revealed only a negligible loss of FITC fluorescence after storage (Figure S2), indicating that surface modifications remained highly stable. In sum, these findings indicated successful acquisition of CM@sEVs from virus-modified CTLA-4@MSCs, supporting their structural and functional integrity.

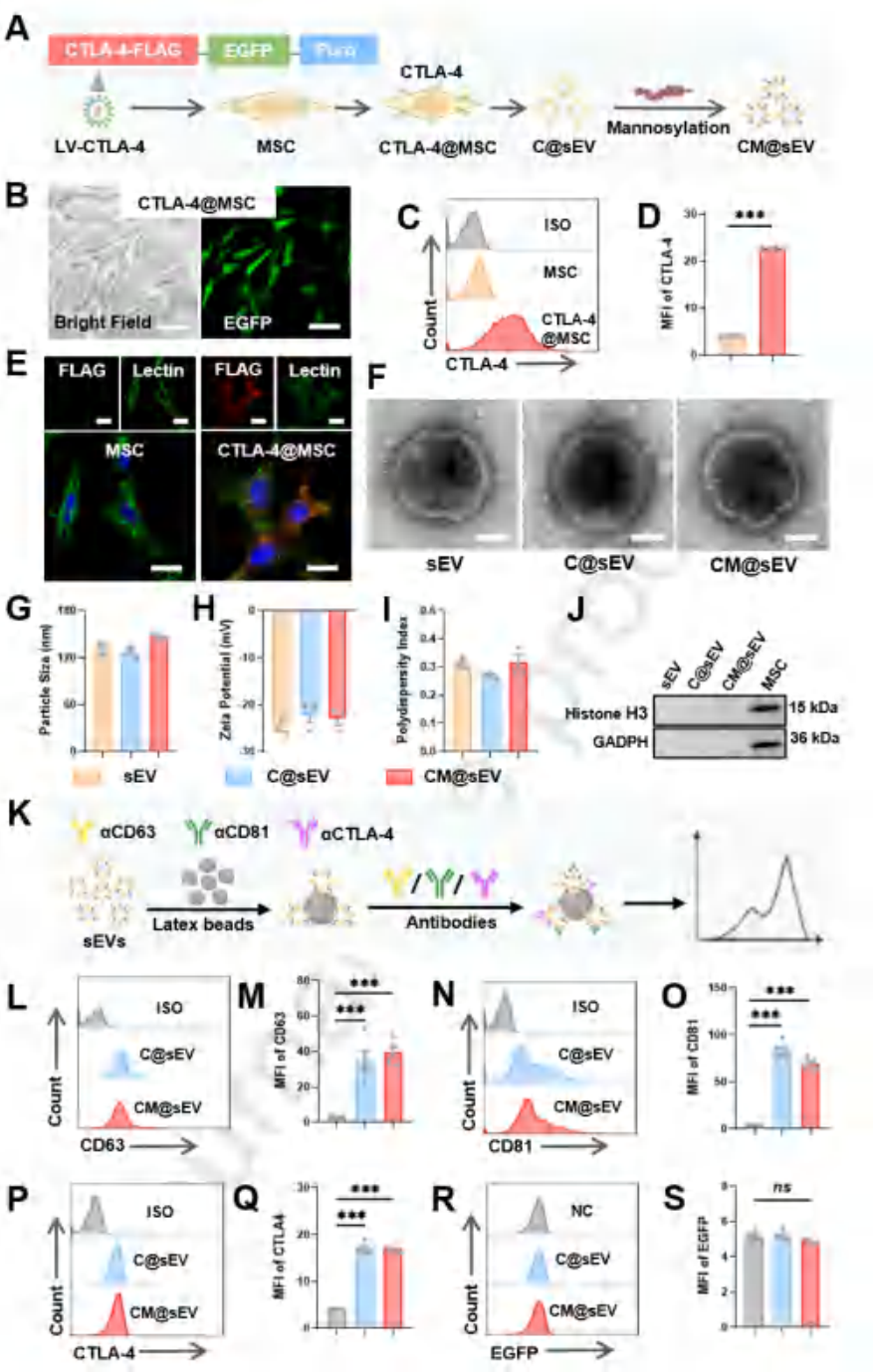

Figure 1. Characterization of CM@sEVs. (A) Schematic representation for CM@sEV generation from CTLA-4@MSCs. (B) Fluorescent microscopy images revealing intracellular EGFP expression in CTLA-4@MSCs. Scale bar, 50 μm. (C&D) Flow validation of CTLA-4 overexpression in CTLA-4@MSCs, along with quantification (n = 5). (E) Co-localization of CTLA-4-FLAG fusion protein with membranous lectin. Scale bar, 20 μm. (F) Characteristic transmission electron microscopy images. Scale bar, 50 nm. (G-I) Particle size, zeta potential, and polydispersity index monitored via dynamic light scattering (n = 3). (J) Immunoblotting for nuclear Histone H3 and cytosolic GAPDH in indicated sEVs. (K-S) Flow validation on aldehyde/sulfate latex bead-captured sEVs. (K) Schematic illustration. (L-S) Expression profiles and quantification for CD63, CD81, CTLA-4, and EGFP (n = 5). P-values were

assessed using one-way ANOVA with Tukey tests or unpaired two-tailed Student's *t*-test. Data are presented as mean ± SEM with error bars. ***$P < 0.001$, *ns* means not significant.

Precise delivery of CM@sEVs to mature DCs

Precise delivery to dendritic cells (DCs) is crucial for effectively disrupting DC-T cell interactions. To achieve this, we functionalized the C@sEV surface with mannose, enhancing its DC specificity [15]. As anticipated, mannosylated C@sEVs (CM@sEVs) exhibited distinct co-localization with dendritic DC2.4 membranes (Figure 2A), suggesting enhanced DC-binding affinity. This DC-targeting specificity was further validated in mature BMDCs using flow cytometry (Figure 2B&C). Notably, this observed binding between CM@sEVs and DCs was dynamically removed in the presence of free mannose (Figure 2A-C), confirming its mannose-dependent nature. To assess cell-type selectivity, flow cytometry of DiD-labeled CM@sEVs revealed differential binding affinities to murine HL-1 cardiomyocytes, MCF fibroblasts, MCEC endothelial cells, and DC2.4 dendritic cells, with DC2.4 exhibiting maximal binding (Figure 2D&E). Collectively, mannose modification significantly enhances DC targeting, which may facilitate suppression of DC-driven inflammatory responses.

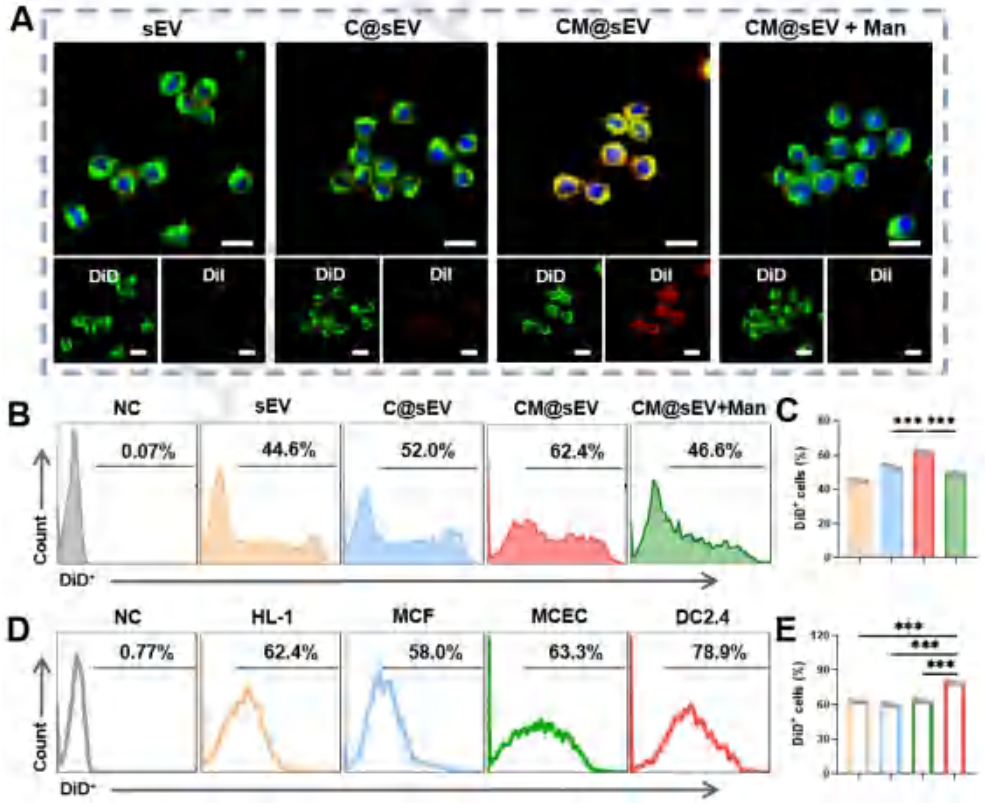

Figure 2. Precise delivery of CM@sEVs to mature DCs. (A) Co-localization of DiI-labeled sEVs with DiD-labeled OVA-activated DC2.4 cell membranes. Scale bar, 20 μm. (B&C) OVA-activated mature BMDCs were cultured with DiD-labeled sEVs (30 μg/mL) for 12 h. For the mannose

competition assay, mBMDCs were primed with free mannose (2 mg/mL) for 1 h before sEV treatment. Histograms and corresponding quantification for DiD fluorescence (n = 5). (D&E) DiD-labeled CM@sEVs (30 μg/mL) were cultured with HL-1, MCF, MCEC, and OVA-activated DC2.4 cells for 12 h. Histograms and corresponding quantification for DiD fluorescence (n = 5). P-values were assessed using one-way ANOVA with Tukey tests. Data are presented as mean ± SEM with error bars. ***P < 0.001.

CM@sEVs abrogate DC-initiated CD8$^+$ T cell priming

Targeting the CD28-CD80/86 co-stimulatory axis via CTLA-4 constitutes a key strategy to disrupt DC-T cell interactions. Although molecular docking confirmed binding configurations for both CD28 and CTLA-4 to CD80/86, notably, CTLA-4 exhibited rather higher affinity for CD80/86 than CD28 (Figure 3A), indicating preferential engagement of CM@sEV-bound CTLA-4 over CD28. To functionally validate this mechanism, we established an in vitro DC/T cell reaction system using CFSE-labeled CD8$^+$ T cells (> 90% purity, Figure S3A&B) and mature BMDCs to assess CM@sEV-mediated mitigation of DC-driven CD8$^+$ T cell over-priming. CD8$^+$ T cell expansion was quantified using a flow-based CFSE fluorescence dilution assay [17]. Of note, CM@sEV treatment significantly suppressed CD8$^+$ T cell expansion (Figure 3B-D). Concurrently, CD8$^+$ T cell activation, assessed by cytokine production, showed a marked reduction in IFN-γ-producing CD8$^+$ T cells post CM@sEV treatment (Figure 3E-G). Additionally, CM@sEVs also markedly suppressed CD8$^+$ T cell expansion in human peripheral blood mononuclear cells (Figure S4A-C). Collectively, these findings underscore the capacity of CM@sEVs to suppress DC-mediated CD8$^+$ T cell priming, positioning it as a noteworthy immunosuppressant.

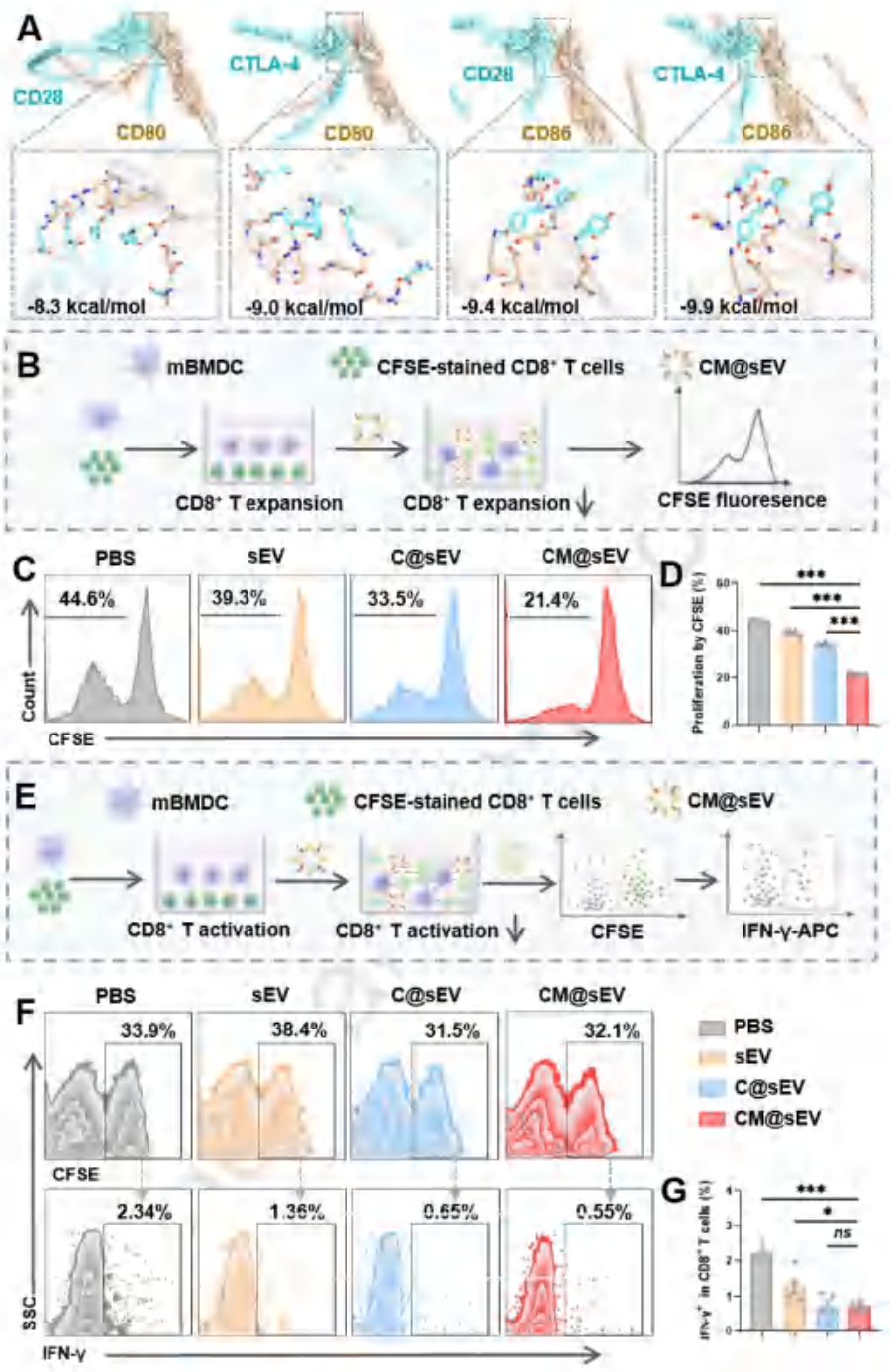

Figure 3. Disrupted DC-driven CD8⁺ T cell priming by CM@sEVs. (A) Molecular docking of CD28/CTLA-4 binding to CD80/86. Lower binding energies indicate a stronger affinity. (B-G) CFSE-labeled CD8⁺ T cells were cultured with OVA-activated mature BMDCs (mBMDCs) and indicated sEVs. (B-D) CD8⁺ T cell proliferation was measured through the CFSE-based dilution assay. (B) Experimental pipeline. (C&D) Histograms and quantification (n = 5). (E-G) CD8⁺ T activation was detected by IFN-γ secretion from CFSE-labeled cells. (E) Experimental outline. (F&G) Histograms and quantification of IFN-γ-releasing CD8⁺ T cells (n = 5). P-values were assessed using one-way ANOVA with Tukey tests. Data are presented as mean ± SEM with error bars. *P < 0.05, ***P < 0.001, *ns* means not significant.

CM@sEVs exert robust *in vivo* therapeutic benefits in ameliorating MI

To explore the therapeutic potential of CM@sEVs in the context of post-MI cardiac repair, treatment was administered intravenously every two days during the initial week (Figure 4A). Functionally, echocardiographic measurements revealed noteworthy enhancements in both ejection fraction (Figure 4B&C for Day 28 post-MI, Figure S5A&B for Day 7 post-MI) and fractional shortening (Figure 4B&D for Day 28 post-MI, Figure S5A&C for Day 7 post-MI) in CM@sEV-treated mice. To define the minimal effective dose of CM@sEVs, a dose-response assessment was performed on Day 28 post-MI. Among the tested doses, the group treated with 100 μg exhibited the highest EF and FS values (Figure S6A-C), thus establishing 100 μg as the minimal effective dose. Morphologically, these functional improvements were paralleled by visibly smaller infarct size (Figure 4E) and reduced relative heart weight (Figure 4F&G). Consistent with functional and morphological observations, histological analysis confirmed a diminished scar area and increased wall thickness post-therapy (Figure 4H-J). Importantly, histopathological examination of the brain, kidney, lung, liver, and spleen revealed minimal structural or cellular changes, with negligible immune infiltration in both groups (Figure S7A). Serum concentrations of alanine aminotransferase, aspartate aminotransferase, blood urea nitrogen, and creatinine demonstrated undetectable hepatotoxicity or nephrotoxicity (Figure S7B-E), supporting the excellent biocompatibility of CM@sEV treatment. Finally, organ distribution analysis revealed predominant CM@sEV accumulation in the liver and spleen (Figure S8). In summary, CM@sEV therapy significantly improves post-MI cardiac function while maintaining *in vivo* biosafety.

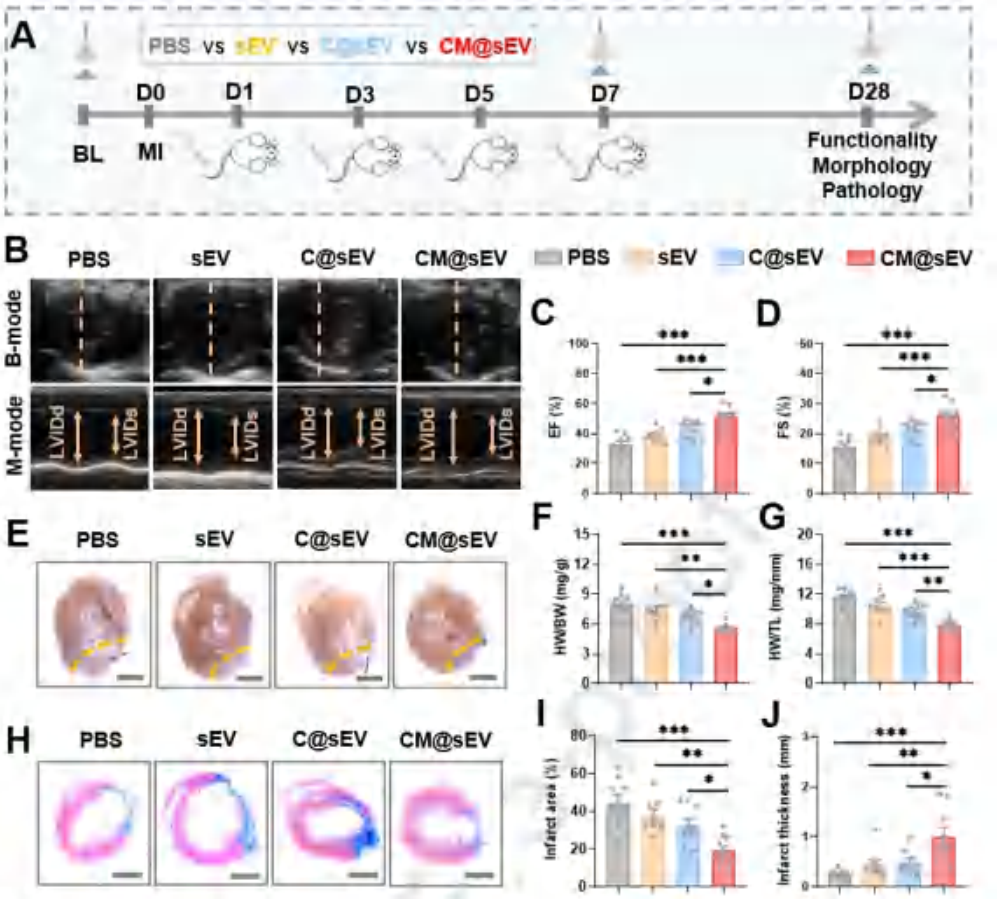

Figure 4. Cardiac repair mediated by CM@sEVs. (A) Schematic timeline illustrating cardio-protection by CM@sEV therapy. (B) B-mode and M-mode echocardiography on Day 28 post-MI, along with arrows denoting left ventricular dimension at systole (LVIDs) and diastole (LVIDd). (C&D) Ejection fraction (EF) and fractional shortening (FS) on Day 28 post-MI (*n* = 9 mice for PBS, C@sEV, and CM@sEV; *n* = 8 mice for sEV). (E-G) Heart morphology and normalized heart weight to body weight (HW/BW) or tibial length (HW/TL) on Day 28 post-MI (*n* = 9 mice for PBS, C@sEV, and CM@sEV; *n* = 8 mice for sEV). Scale bar, 2 mm. (H) Masson's trichrome staining displaying fibrotic tissue (blue) on Day 28 post-MI. Scale bar, 2 mm. (I&J) Quantification of infarct area and thickness via Masson's trichrome staining (*n* = 9 mice for PBS, C@sEV, and CM@sEV; *n* = 8 mice for sEV). *P*-values were assessed using one-way ANOVA with Tukey tests. Data are presented as mean ± SEM with error bars. **P* < 0.05, ***P* < 0.01, ****P* < 0.001.

Immunosuppression on T-cell profiling by CM@sEVs

Prior investigations have established that cytotoxic $CD8^+$ T lymphocytes become activated following MI, contributing to ischemic immunopathology. We therefore evaluated T cell behavior post-therapy in our current study (Figure 5A). Flow cytometry analysis unveiled a notable reduction in $CD8^+$ T cell population following CM@sEV therapy (Figure 5B&C). Since activated $CD8^+$ T cells

serve as a primary source for pro-inflammatory cytokines, we further investigated their functional response. Our results demonstrated a marked decline in IFN-γ- (Figure 5D&E) and Granzyme B-producing $CD8^+$ T cells (Figure 5F&G), indicating compromised T cell functionality. Additionally, the proportion of $CD4^+$ helper T lymphocytes was substantially suppressed, with the lowest percentage observed in CM@sEV-treated mice (Figure S9A&B). Conversely, immunosuppressive regulatory T cells (Tregs), known to benefit cardiac repair [18], were elevated in response to CM@sEV therapy (Figure S9C&D). Taken together, these data suggest that CM@sEV immunotherapy effectively suppresses $CD8^+$ T cell hyperactivation and calms ischemic hyper-inflammation.

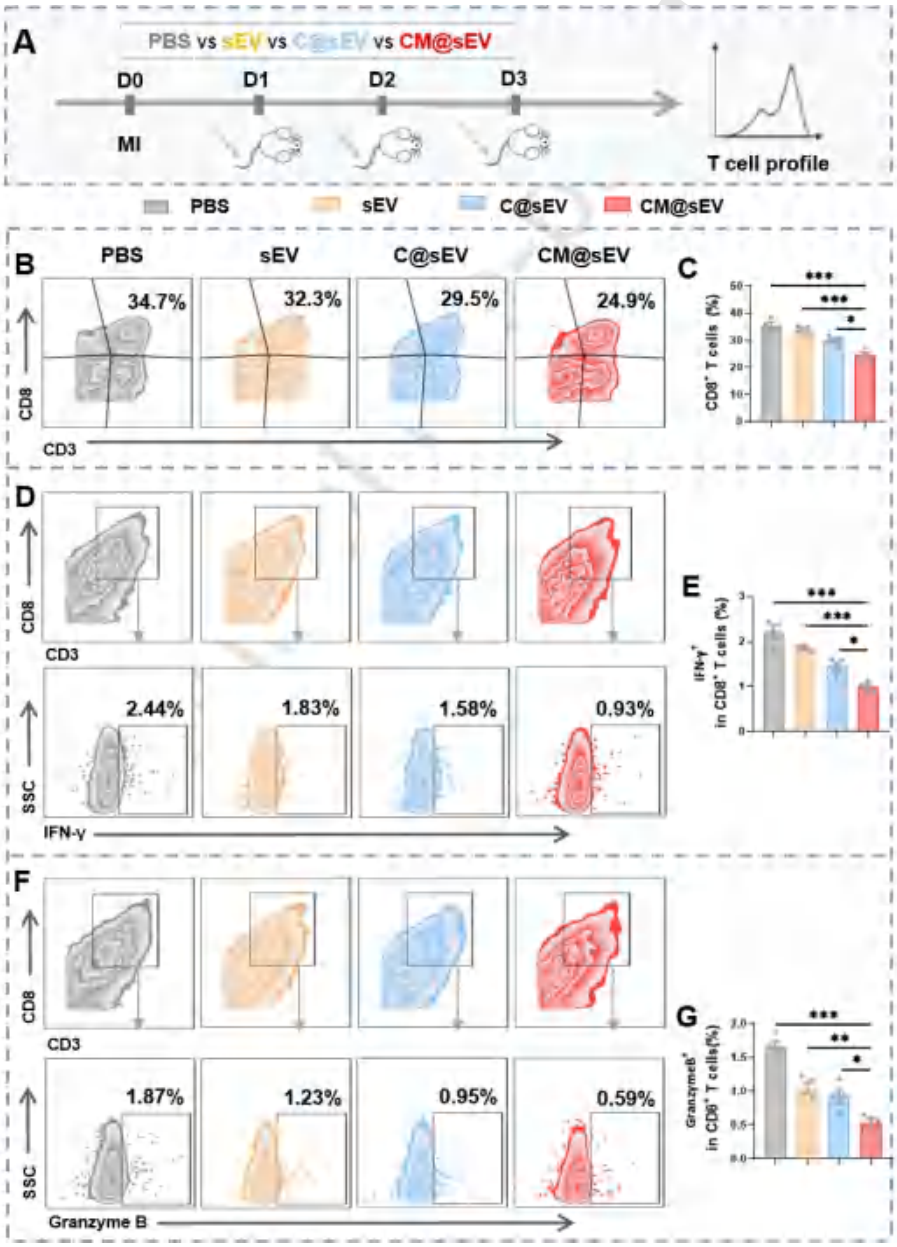

Figure 5. *In vivo* modulation of T-cell dynamics by CM@sEVs. (A) Experimental outline for profiling T cells by CM@sEVs. (B&C) Zebra plots and quantification for splenic $CD8^+$ T cell

($CD3^+CD8^+$) population (n = 4). (D-G) Dot plots and quantitation for splenic IFN-γ- and Granzyme B-secreting $CD8^+$ T cells (n = 4). P-values were assessed using one-way ANOVA with Tukey tests. Data are presented as mean ± SEM with error bars. *P < 0.05, **P < 0.01, ***P < 0.001.

CM@sEVs regulate *in vivo* $CD8^+$ T transcriptome

To further elucidate the immunoregulatory perspective of CM@sEVs, a genome-wide transcriptome was performed on $CD8^+$ T cells *in vivo* (Figure 6A). Among the 181 differentially expressed genes, 99 were downregulated and 82 upregulated (Figure 6B). Despite distinct mRNA expression profiles between groups (Figure 6C), several key genes related to inflammation or cell proliferation, including matrix metalloproteinase-13 (*MmP13*), pleckstrin 2 (*Plek2*), and vasorin (*Vasn*), were further validated (Figure 6D). Specifically, *Mmp13* overexpression is linked to NF-kB activation and pro-inflammatory cytokine production [19], *Plek2* drives cell proliferation through AKT signaling [20], and V*asn* deficiency elevates inflammatory cytokine production [21]. KEGG pathway enrichment analysis highlighted significant enrichment in pathways related to the immune system, cell growth and death, viral infectious diseases, and cardiovascular diseases (Figure 6E). Specifically, IL-17 signaling and Th17 cell differentiation pathways were prominently enriched (Figure S10A-D). In parallel, gene ontology (GO) analysis of $CD8^+$ lymphocytes identified the top 10 enriched terms, predominantly linked to immune activation and regulation (Figure 6F). Gene set enrichment analysis further revealed significant suppression of DNA replication, inflammatory response, and cell activation following CM@sEV treatment (Figure 6G-I). Collectively, these findings underscore that CM@sEVs effectively dampen $CD8^+$ T cell activation, thereby exerting potent immunomodulatory effects.

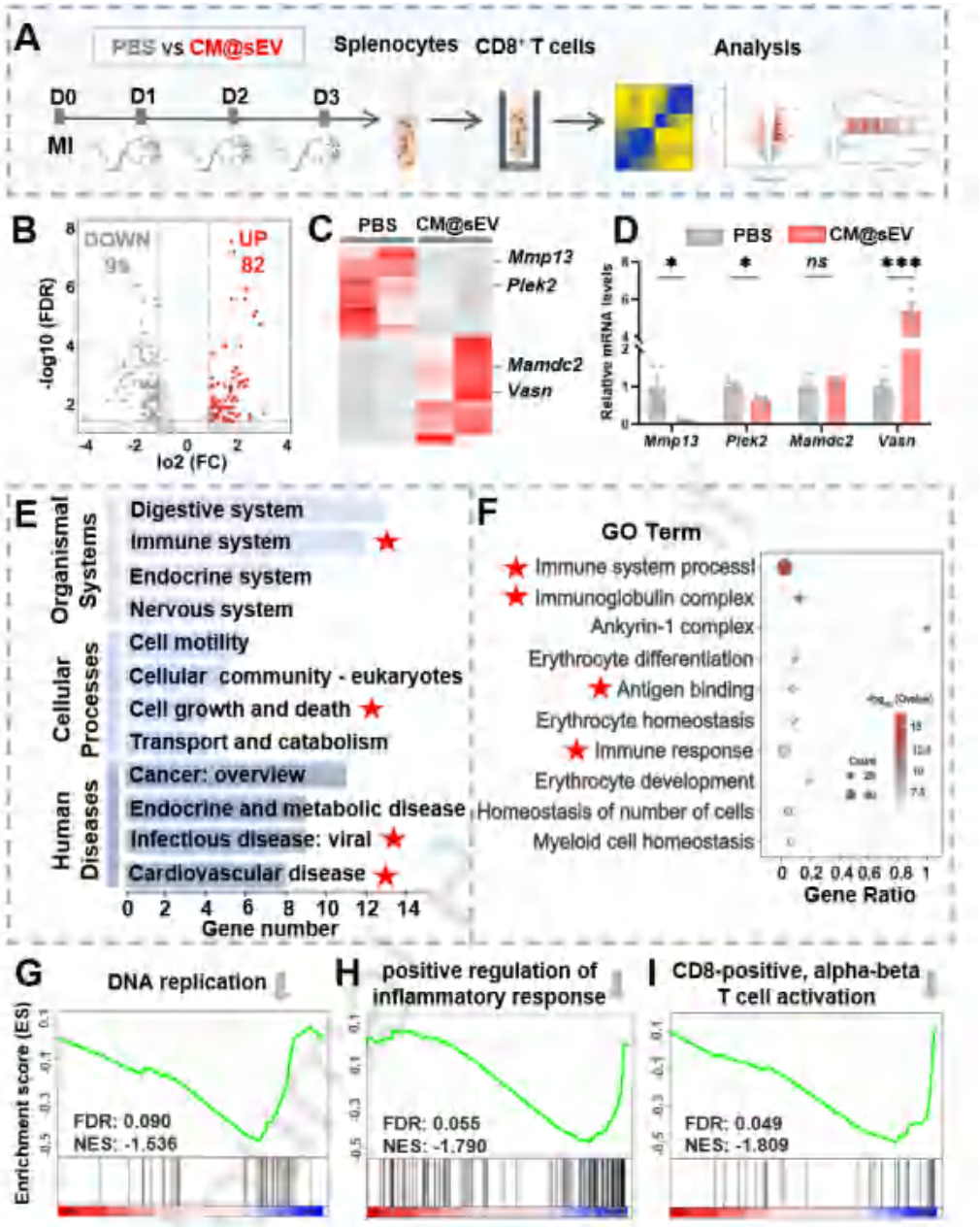

Figure 6. *In vivo* regulation of CD8⁺ T transcriptome by CM@sEVs. (A) Schematic design for *in vivo* RNA-seq analysis on Day 3 post-MI. (B&C) Volcano and heatmap plots of up- and downregulated genes between PBS and CM@sEV groups. (D) mRNA validation of selected RNAseq genes (n = 4). (E&F) Kyoto Encyclopedia of Genes and Genomes (KEGG) and Gene Ontology (GO) enrichment for significantly differential genes. (G-I) Gene set enrichment analysis (GSEA) for key dysregulated pathways. FDR, false discovery rate; NES, normalized enrichment score. *P*-values were assessed using unpaired two-tailed Student's *t*-test. Data are presented as mean ± SEM with error bars. *$P < 0.05$, ***$P < 0.001$, *ns* means not significant.

Cardioprotective benefits of CM@sEVs are mediated via counteracting CD8⁺ T cell activation

To elucidate whether the cardioprotective effects of CM@sEVs are mediated through CD8⁺ T cell suppression, we employed co-stimulatory CD28 antibody (aCD28) to revive those hypofunctional

and exhausted T cells (Figure 7A). As illustrated in Figure 7B, aCD28 was administered simultaneously with CM@sEVs at specific intervals, followed by assessments regarding cardiac functionality, morphology, and pathology. Notably, echocardiography on Day 28 post-MI demonstrated significant cardioprotection following CM@sEV therapy, which was substantially reduced by concurrent aCD28 administration (Figure 7C-E for Day 28 post-MI; Figure S11A-C for Day 7 post-MI). This reduced cardioprotective effect was further corroborated by elevated infarct size (Figure 7F, I-K) and relative heart weight (Figure 7G&H) in the CM@sEV plus aCD28 group, suggesting exacerbated pathological remodeling and hypertrophy. In summary, our findings strongly indicate that the cardioprotective efficacy of CM@sEV therapy is mediated by activity suppression via $CD8^+$ cytotoxic T cells.

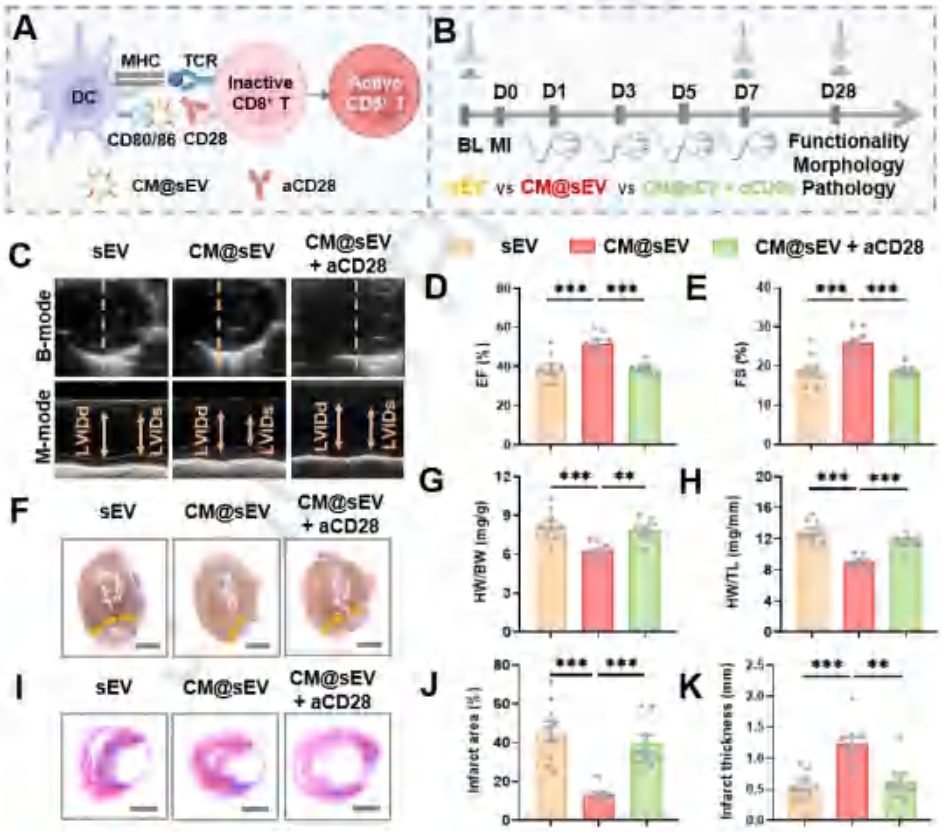

Figure 7. $CD8^+$ T lymphocyte activation abrogates cardioprotective effects of CM@sEVs. (A) Schematic illustration for sustained $CD8^+$ T lymphocyte activation induced by aCD28. (B) Experimental timeline. (C) B-mode and M-mode echocardiography on Day 28 post-MI, along with arrows denoting LVIDs and LVIDd. (D&E) Quantification of EF and FS on Day 28 post-MI (*n* = 9 mice for sEV and CM@sEV; *n* = 8 mice for CM@sEV + aCD28). (F-H) Heart morphology and heart weight/body weight (HW/BW) or tibial length (HW/TL) ratio on Day 28 post-MI (*n* = 9 mice for sEV and CM@sEV; *n* = 8 mice for CM@sEV + aCD28). Scale bar, 2 mm. (I) Masson's trichrome

staining showing fibrotic tissue (blue) and healthy myocardium (red). Scale bar, 2 mm. (J&K) Quantification of infarct area and thickness (n = 9 mice for sEV and CM@sEV; n = 8 mice for CM@sEV + aCD28). P-values were assessed using one-way ANOVA with Tukey tests. Data are presented as mean ± SEM with error bars. $^{**}P < 0.01$, $^{***}P < 0.001$.

Conclusion

In summary, mannosylated CTLA-4-presenting sEVs (CM@sEVs) were developed for myocardial infarction (MI) therapy. These vesicles disrupt CD80/86-CD28 co-stimulatory signaling, impairing dendritic cell (DC)-mediated $CD8^+$ T cell priming, thus alleviating ischemic immunopathology and promoting myocardial repair. In contrast to conventional T cell-modulating therapies, CM@sEVs directly modulate T cell dynamics via DC-dependent mechanisms, providing a straightforward, stable, and secure approach for treating ischemic cardiomyopathy.

Material and methods

Cell culture and treatment

Immature bone marrow-derived dendritic cells (imBMDCs), also from C57BL/6 mice, were maintained in RPMI 1640 together with interleukin-4 (Novoprotein, CK15, 10 ng/mL) plus GM-CSF (Yeasen, 91108ES08, 20 ng/mL). To induce maturation, imBMDCs were exposed to 30 μg/mL ovalbumin (OVA) (Sangon Biotech, T510212-0001) for 24 h. Mesenchymal stem cells (MSCs) derived from C57BL/6 bone marrow (Cyagen Biosciences) were cultured in DMEM/F12 medium (PrIcella) and phenotypically validated via markers CD29, CD45, CD11b, and CD117 [22]. Peripheral blood mononuclear cells (PBMCs) were collected from healthy volunteers following informed consent and commercially sourced through Milestone Biological Science & Technology Co., Ltd. DC2.4 murine dendritic cells were cultivated in RPMI 1640 (Dakewe, 6016011) enriched with FBS (ExCell Bio) and Penicillin-Streptomycin (Cyagen, ATPS-10001-100); HL-1 cells (Otwo Biotech) were similarly cultured in high-glucose DMEM (Procell) with equivalent supplements. For primary cells, neonatal mouse cardiac fibroblasts were isolated and cultured using our established protocol [23]. Murine splenic $CD8^+$ T lymphocytes were collected using MojoSort Mouse CD8 T Cell Isolation Kit.

Generation and maintenance of CTLA-4@MSCs

Lentivirus encoding EGFP and murine CTLA-4 with a C-terminal FLAG tag (pSSFV-CTLA-4-FLAG-E2A-EGFP-pSV40-puromycin) was ordered from GeneChem, China (GV643). To optimize lentiviral transduction efficiency, 5 μg/mL of Polybrene (APExBIO, K2701) was supplemented. Following

transduction, CTLA-4@MSCs were maintained under 3 μg/mL puromycin (Solarbio, IP1280) to ensure stable transgene integration [24].

Preparation and characterization of CM@sEVs

FBS intended for sEV production was depleted of bovine EVs by ultra-centrifugation at 110,000 × g for 8 h [25]. For sEV collection, the cell culture medium was sequentially cleared of cellular debris and subjected to ultracentrifugation at 110,000 × g [26]. To generate mannosylated C@sEVs (CM@EVs), C@EVs were stirred with DSPE-PEG2000-Mannose (0.1 mg/mL) for membrane incorporation. Size distribution, zeta potential, and polydispersity index were monitored via Zetasizer Nano ZS (Malvern, ZEN3600). Transmission Electron Microscopy (JEM1400, JEOL) was conducted by Wuhan MISP Bio-technology Co., Ltd.

***In silico* molecular docking**

For in silico molecular docking, binding models of CD80/86 with target proteins were predicted by AlphaFold3 (https://alphafoldserver.com/). Binding free energies were quantitatively assessed via PRODIGY (https://rascar.science.uu.nl/prodigy/), while molecular visualization and interaction analyses were conducted using PyMOL.

DC/T cell co-culture system for $CD8^+$ T expansion and activation

In our DC/T cell co-culture system, CFSE-labeled $CD8^+$ T lymphocytes [17, 27] were initially mixed with OVA-activated mBMDCs at a 5:1 ratio for 24 h before sEV supplement (100 μg/mL) for another 72 h. T cell proliferation was measured by CFSE dilution, while their activation was monitored via IFN-γ secretion in CFSE-labeled cells.

Flow cytometry

For intracellular antibody staining, cells were fixed and permeabilized using the Fix & Perm Kit (MultiSciences, 70-GAS006/2) before antibody labeling. For surface antibody staining, cells were incubated in staining buffer with indicated fluorescent antibodies. Flow cytometry data were acquired on Millipore Guava easyCyte [28]. Detailed antibody information is provided in Table S1.

Myocardial infarction and *in vivo* safety evaluation

All animal studies received approval from the Animal Ethics Committee of Soochow University (SUDA20240911A31). Mice were accommodated in individually ventilated cages under standardized environmental conditions. MI was induced via left coronary artery ligation using 6-0 silk sutures. Successful infarction was confirmed by visible blanching of the affected myocardium.

For CD28 constitutive activation, aCD28 (20 μg/injection, Selleck, A2108) was administered via tail vein injection.

Serum concentrations of aspartate aminotransferase and alanine aminotransferase were employed as indicators for hepatic toxicity, while urea nitrogen and creatinine levels for renal toxicity [29]. For organ pathology, liver, kidney, lung, spleen, and brain sections on Day 28 post-injection were H&E-stained by ZuoChengBio Co.

Echocardiography and Masson's trichrome staining

Murine heart function was evaluated using the Vevo 2100 high-frequency ultrasound system (VisualSonics) with B-mode and M-mode images [27, 30]. To visualize collagen deposition, ischemic heart sections were stained with Masson's trichrome [31, 32]. Infarct area and thickness were quantified using ImageJ software.

***In vivo* biodistribution analysis**

MI mice were intravenously injected with 300 μg of DiR-labeled CM@sEVs via the tail vein. Subsequently, major organs (liver, spleen, kidney, and heart) were collected for ex vi*vo* imaging 48 h post-injection. DiR fluorescence was quantified using an IVIS Spectrum imaging system (PerkinElmer).

Immunofluorescence and immunoblotting

Cells were fixed with 4% Paraformaldehyde Solution and blocked with 3% BSA plus 0.3% Triton X-100. Stained cells were mounted with DAPI-containing anti-fade solution (KeyGEN BioTECH, KGA1523) and imaged with a Zeiss LSM880 confocal microscope [23, 33].

Protein extraction was accomplished using RIPA lysis buffer plus Protease Inhibitor Cocktail (CoWin, CW2200S) [34]. Antibodies were diluted in NCM Universal Antibody Diluent (New Cell & Molecular Biotech, WB500D). Immunoreactivity was detected using the Omni-ECL Femto Light Chemiluminescence Kit (EpiZyme, SQ201) [35]. Detailed antibody information is described in Table S1.

RNA extraction and RT-quantitative PCR

RNA was isolated using Super FastPure Cell RNA Isolation Kit (Vazyme, RC102). Complementary DNA was synthesized with HiScript IV RT SuperMix for qPCR (+gDNA wiper, Vazyme, R423-01), and gene expression was analyzed via Hieff UNICON Universal Blue qPCR SYBR Green Master Mix (Yeasen, 11184ES03) [36, 37]. *18S* was used to normalize gene expression. The following primers

were used: *MmP13* (sense: 5'-GAT GAC CTG TCT GAG GAA GAC C-3', antisense: 5'-GCA TTT CTC GGA GCC TGT CAA C-3'); *Plek2* (sense: 5'-GCT GAG CAG TTT CTG GAT GAC TC-3', antisense: 5'-GGT AGC CTT GTT TGA CCA CTG TG-3'); *Mamdc2* (sense: 5'-TGG GAC AAG GAA ACA CGG CTA G-3', antisense: 5'-TTC CAG CGG TTC ACA AAG CCA C-3'); and *Vasn* (sense: 5'-CCA GCA TCC ATC TGC CTG AAT G-3', antisense: 5'-CTT GCT CCA CTG GAC TCT CAC A-3').

Genome-wide RNA-seq transcriptome

To perform RNA-seq transcriptome, splenic $CD8^+$ T lymphocytes were isolated and subjected to RNA extraction, mRNA enrichment, and subsequent reverse transcription. RNA-seq transcriptome was conducted on the Illumina Novaseq 6000 platform (Gene Denovo Biotechnology) [38]. Data analysis was performed via Omicsmart (http://www.omicsmart.com). Differentially expressed genes (DEGs) were identified as absolute fold change > 2 and false discovery rate < 0.05.

Statistical analyses

Multiple comparisons were conducted by one-way or two-way ANOVA, while comparisons between two groups were calculated via unpaired Student's *t*-test. Statistical analyses were conducted using GraphPad Prism, with $P < 0.05$ considered statistically significant. Unless stated otherwise, all results were presented as mean ± SEM.

Acknowledgments

This work was supported by the National Natural Science Foundation of China (82070363, 92168203), National Key R&D Program of China (2022YFA1104300), Jiangsu Cardiovascular Medicine Innovation Center (CXZX202210), Boxi Youth Natural Science Foundation (BXQN2023016), and Priority Academic Program Development of Jiangsu Higher Education Institutions. We appreciate the technical support by "Zhongke e-Test Research Service, www.zkec.cc".

Consent for publication

All authors have approved the manuscript's content and its publication.

Conflicts of interest

Authors' declaration: No conflicts of interest exist.

Data availability

For accessibility, raw sequencing data have been deposited in the Genome Sequence Archive (CRA022020) at the BIG Data Center, Beijing Institute of Genomics (BIG), Chinese Academy of Sciences (https://bigd.big.ac.cn/).

References

1. Tsao CW, Aday AW, Almarzooq ZI, Anderson CAM, Arora P, Avery CL, Baker-Smith CM, Beaton AZ, Boehme AK, Buxton AE *et al*: **Heart Disease and Stroke Statistics-2023 Update: A Report From the American Heart Association**. *Circulation* 2023, **147**(8):e93-e621.
2. Tang Q, Li M, Wang S, Li J, Cao S, Liu H, Wu Y, Chen Y, Shen H, Zhang W *et al*: **Room-temperature-stable immunosuppressive nanovesicles for mitigating immunopathology and streamlining cardioprotection post-infarction**. *Chem Eng J* 2024, **500**:157030.
3. Santos-Zas I, Lemarié J, Zlatanova I, Cachanado M, Seghezzi JC, Benamer H, Goube P, Vandestienne M, Cohen R, Ezzo M *et al*: **Cytotoxic CD8(+) T cells promote granzyme B-dependent adverse post-ischemic cardiac remodeling**. *Nat Commun* 2021, **12**(1):1483.
4. Liu C, Liu X, Xiang X, Pang X, Chen S, Zhang Y, Ren E, Zhang L, Liu X, Lv P *et al*: **A nanovaccine for antigen self-presentation and immunosuppression reversal as a personalized cancer immunotherapy strategy**. *Nat Nanotechnol* 2022, **17**(5):531-540.
5. Schwartz JC, Zhang X, Fedorov AA, Nathenson SG, Almo SC: **Structural basis for co-stimulation by the human CTLA-4/B7-2 complex**. *Nature* 2001, **410**(6828):604-608.
6. Stamper CC, Zhang Y, Tobin JF, Erbe DV, Ikemizu S, Davis SJ, Stahl ML, Seehra J, Somers WS, Mosyak L: **Crystal structure of the B7-1/CTLA-4 complex that inhibits human immune responses**. *Nature* 2001, **410**(6828):608-611.
7. Krummel MF, Allison JP: **CD28 and CTLA-4 have opposing effects on the response of T cells to stimulation**. *J Exp Med* 1995, **182**(2):459-465.
8. Chen L: **Co-inhibitory molecules of the B7-CD28 family in the control of T-cell immunity**. *Nat Rev Immunol* 2004, **4**(5):336-347.
9. Zhang W, Campbell DH, Walsh BJ, Packer NH, Liu D, Wang Y: **Cancer-derived small extracellular vesicles: emerging biomarkers and therapies for pancreatic ductal adenocarcinoma diagnosis/prognosis and treatment**. *J Nanobiotechnology* 2022, **20**(1):446.
10. Fang T, Li B, Li M, Zhang Y, Jing Z, Li Y, Xue T, Zhang Z, Fang W, Lin Z *et al*: **Engineered Cell Membrane Vesicles Expressing CD40 Alleviate System Lupus Nephritis by Intervening B Cell Activation**. *Small Methods* 2023, **7**(3):e2200925.
11. Zhang F, Guo J, Zhang Z, Duan M, Wang G, Qian Y, Zhao H, Yang Z, Jiang X: **Application of engineered extracellular vesicles for targeted tumor therapy**. *J Biomed Sci* 2022, **29**(1):14.
12. Chen X, Luo Y, Zhu Q, Zhang J, Huang H, Kan Y, Li D, Xu M, Liu S, Li J *et al*: **Small extracellular vesicles from young plasma reverse age-related functional declines by improving mitochondrial energy metabolism**. *Nat Aging* 2024, **4**(6):814-838.
13. Conniot J, Scomparin A, Peres C, Yeini E, Pozzi S, Matos AI, Kleiner R, Moura LIF, Zupančič E, Viana AS *et al*: **Immunization with mannosylated nanovaccines and inhibition of the immune-suppressing microenvironment sensitizes melanoma to immune checkpoint modulators**. *Nat Nanotechnol* 2019, **14**(9):891-901.
14. Zeng JY, Lingesh S, Krishnan NB, Loong BSY, Liu M, Chen Q, Yang YY: **Cholesterol-Derived Mannosylated Polypeptide-Formed Lipid Nanoparticles for Efficient in Vivo mRNA Delivery**. *Small Methods* 2025, **9**(6):e2401712.
15. Yang R, Xu J, Xu L, Sun X, Chen Q, Zhao Y, Peng R, Liu Z: **Cancer Cell Membrane-Coated Adjuvant Nanoparticles with Mannose Modification for Effective Anticancer Vaccination**. *ACS Nano* 2018, **12**(6):5121-5129.
16. Lei J, Qi S, Yu X, Gao X, Yang K, Zhang X, Cheng M, Bai B, Feng Y, Lu M *et al*: **Development of**

Mannosylated Lipid Nanoparticles for mRNA Cancer Vaccine with High Antigen Presentation Efficiency and Immunomodulatory Capability. *Angew Chem Int Ed Engl* 2024, **63**(13):e202318515.

17. Hawkins ED, Hommel M, Turner ML, Battye FL, Markham JF, Hodgkin PD: **Measuring lymphocyte proliferation, survival and differentiation using CFSE time-series data**. *Nat Protoc* 2007, **2**(9):2057-2067.
18. Kvakan H, Kleinewietfeld M, Qadri F, Park JK, Fischer R, Schwarz I, Rahn HP, Plehm R, Wellner M, Elitok S *et al*: **Regulatory T cells ameliorate angiotensin II-induced cardiac damage**. *Circulation* 2009, **119**(22):2904-2912.
19. Horváth E, Sólyom Á, Székely J, Nagy EE, Popoviciu H: **Inflammatory and Metabolic Signaling Interfaces of the Hypertrophic and Senescent Chondrocyte Phenotypes Associated with Osteoarthritis**. *Int J Mol Sci* 2023, **24**(22):16468.
20. Han X, Mei Y, Mishra RK, Bi H, Jain AD, Schiltz GE, Zhao B, Sukhanova M, Wang P, Grigorescu AA *et al*: **Targeting pleckstrin-2/Akt signaling reduces proliferation in myeloproliferative neoplasm models**. *J Clin Invest* 2023, **133**(6):e159638.
21. Guo X, Sun J, Liang J, Zhu S, Zhang M, Yang L, Huang X, Xue K, Mo Z, Wen S *et al*: **Vasorin contributes to lung injury via FABP4-mediated inflammation**. *Mol Biol Rep* 2022, **49**(10):9335-9344.
22. Chen W, Wang S, Xia J, Huang Z, Tu X, Shen Z: **Protein phosphatase 2A plays an important role in migration of bone marrow stroma cells**. *Mol Cell Biochem* 2016, **412**(1-2):173-180.
23. Zhou W, Jiang X, Tang Q, Ding L, Xiao W, Li J, Wu Y, Ruan HB, Shen Z, Chen W: **Glucosamine facilitates cardiac ischemic recovery via recruiting Ly6C(low) monocytes in a STAT1 and O-GlcNAcylation-dependent fashion**. *Clin Transl Med* 2022, **12**(3):e762.
24. Liu H, Li M, Xiang B, Yang Z, Cao S, Gong W, Li J, Zhou W, Ding L, Tang Q *et al*: **An integrated "Engage & Evasion" approach for mononuclear phagocyte system escape and efficient extracellular vesicle therapy**. *J Nanobiotechnol* 2024, **22**(1):770.
25. Ding L, Zhou W, Zhang J, Tang Q, Xiao W, Chen M, Shen Z, Chen W: **Calming egress of inflammatory monocytes and related septic shock by therapeutic CCR2 silencing using macrophage-derived extracellular vesicles**. *Nanoscale* 2022, **14**(13):4935-4945.
26. Chen M, Wang S, Chen Y, Shen H, Chen L, Ding L, Tang Q, Yang Z, Chen W, Shen Z: **Precision cardiac targeting: empowering curcumin therapy through smart exosome-mediated drug delivery in myocardial infarction**. *Regen Biomater* 2024, **11**:rbad108.
27. Zhou W, Tang Q, Wang S, Ding L, Chen M, Liu H, Wu Y, Xiong X, Shen Z, Chen W: **Local thiamet-G delivery by a thermosensitive hydrogel confers ischemic cardiac repair via myeloid M2-like activation in a STAT6 O-GlcNAcylation-dependent manner**. *Int Immunopharmacol* 2024, **131**:111883.
28. Chen W, Gu P, Jiang X, Ruan H-B, Li C, Gao X: **Protein phosphatase 2A catalytic subunit α (PP2Acα) maintains survival of committed erythroid cells in fetal liver erythropoiesis through the STAT5 pathway**. *Am J Pathol* 2011, **178**(5):2333-2343.
29. Gao M, Li Y, Ho W, Chen C, Chen Q, Li F, Tang M, Fan Q, Wan J, Yu W *et al*: **Targeted mRNA Nanoparticles Ameliorate Blood-Brain Barrier Disruption Postischemic Stroke by Modulating Microglia Polarization**. *ACS Nano* 2024, **18**(4):3260-3275.
30. Zeng Y, Liao X, Guo Y, Liu F, Bu F, Zhan J, Zhang J, Cai Y, Shen M: **Baicalin-peptide supramolecular self-assembled nanofibers effectively inhibit ferroptosis and attenuate doxorubicin-induced**

cardiotoxicity. *J Control Release* 2024, **366**:838-848.

31. Zhao P, Zhou W, Zhang Y, Li J, Zhao Y, Pan L, Shen Z, Chen W, Hui J: **Aminooxyacetic acid attenuates post-infarct cardiac dysfunction by balancing macrophage polarization through modulating macrophage metabolism in mice**. *J Cell Mol Med* 2020, **24**(4):2593-2609.
32. Wang Y, Meng D, Shi X, Hou Y, Zang S, Chen L, Spanos M, Li G, Cretoiu D, Zhou Q *et al*: **Injectable hydrogel with miR-222-engineered extracellular vesicles ameliorates myocardial ischemic reperfusion injury via mechanotransduction**. *Cell Rep Med* 2025, **6**(3):101987.
33. Yang J, Li S, Li Z, Yao L, Liu M, Tong KL, Xu Q, Yu B, Peng R, Gui T *et al*: **Targeting YAP1-regulated Glycolysis in Fibroblast-Like Synoviocytes Impairs Macrophage Infiltration to Ameliorate Diabetic Osteoarthritis Progression**. *Adv Sci (Weinh)* 2024, **11**(5):e2304617.
34. Wu J, Dong Y, Teng X, Cheng M, Shen Z, Chen W: **Follistatin-like 1 attenuates differentiation and survival of erythroid cells through Smad2/3 signaling**. *Biochem Biophys Res Commun* 2015, **466**(4):711-716.
35. Chen W, Xia J, Hu P, Zhou F, Chen Y, Wu J, Lei W, Shen Z: **Follistatin-like 1 protects cardiomyoblasts from injury induced by sodium nitroprusside through modulating Akt and Smad1/5/9 signaling**. *Biochem Biophys Res Commun* 2016, **469**(3):418-423.
36. Wu J, Wang J, Zeng X, Chen Y, Xia J, Wang S, Huang Z, Chen W, Shen Z: **Protein phosphatase 2A regulatory subunit B56β modulates erythroid differentiation**. *Biochem Biophys Res Commun* 2016, **478**(3):1179-1184.
37. Zhang YL, Bai J, Yu WJ, Lin QY, Li HH: **CD11b mediates hypertensive cardiac remodeling by regulating macrophage infiltration and polarization**. *J Adv Res* 2024, **55**:17-31.
38. Wu W, Guo H, Jing D, Zhang Z, Zhang Z, Pu F, Yang W, Jin X, Huang X, Shao Z: **Targeted Delivery of PD-L1-Derived Phosphorylation-Mimicking Peptides by Engineered Biomimetic Nanovesicles to Enhance Osteosarcoma Treatment**. *Adv Healthc Mater* 2022, **11**(23):e2200955.

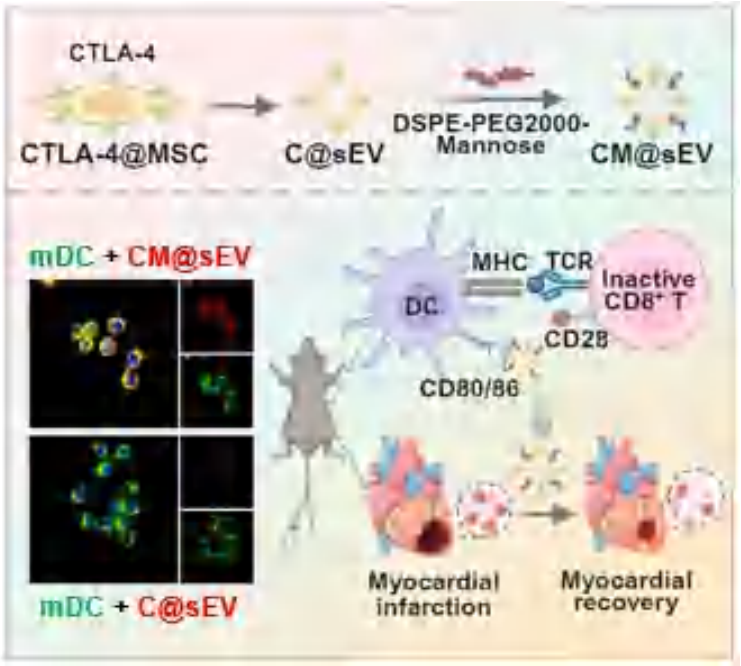

Graphical abstract. Mannosylated CTLA-4-presenting small extracellular vesicles (CM@sEVs) were engineered to specifically disrupt CD80/86-CD28 costimulatory interaction, thereby inhibiting dendritic cell (DC)-mediated $CD8^+$ T cell priming. Through their targeted binding to mature DC membranes, these CM@sEVs potently modulate *in vivo* T-cell dynamics, concurrently calming ischemic hyper-inflammation and promoting myocardial recovery. Created in BioRender. Shengnan, W. (2025) https://BioRender.com/zuvkpo1.

Highlights

- Mannosylation enables precise DC delivery via receptor-specific interactions.
- CM@sEVs suppress DC-driven $CD8^+$ T cell priming by blocking CD80/86-CD28 axis.
- CM@sEVs calm ischemic hyper-inflammation via reshaping *in vivo* T-cell dynamics.
- CM@sEVs benefit myocardial recovery by disrupting post-ischemic immunopathology.